PHYSICAL REVIEW B **93**, 081407(R) (2016)

Determination of scattering time and of valley occupation in transition-metal dichalcogenides doped by field effect

Thomas Brumme* and Matteo Calandra
CNRS, UMR 7590, Sorbonne Universités, UPMC Univ Paris 06, IMPMC - Institut de Minéralogie, de Physique des Matériaux, et de Cosmochimie, 4 place Jussieu, F-75005, Paris, France

Francesco Mauri
Dipartimento di Fisica, Università di Roma La Sapienza, Piazzale Aldo Moro 5, I-00185 Roma, Italy
(Received 10 December 2015; published 12 February 2016)

The transition-metal dichalcogenides have attracted a lot of attention as a possible stepping-stone toward atomically thin and flexible field-effect transistors. One key parameter to describe the charge transport is the time between two successive scattering events—the transport scattering time. In a recent report, we have shown that it is possible to use density functional theory to obtain the band structure of two-dimensional semiconductors in the presence of field effect doping. Here, we report a simple method to extract the scattering time from the experimental conductivity and from the knowledge of the band structure. We apply our approach to monolayers and multilayers of MoS_2, $MoSe_2$, $MoTe_2$, WS_2, and WSe_2 in the presence of a gate. In WS_2, for which accurate measurements of mobility have been published, we find that the scattering time is inversely proportional to the density of states at the Fermi level. Finally, we show that it is possible to identify the critical doping at which different valleys start to be occupied from the doping dependence of the conductivity.

DOI: 10.1103/PhysRevB.93.081407

The discovery of graphene [1] has also led to an ever-growing interest in other two-dimensional (2D) materials such as monolayers or few-layer systems (nanolayers) of transition-metal dichalcogenides [2,3] (TMDs). TMDs form layered structures like graphene in which the different layers are held together by weak van der Waals forces (cf. Fig. 1). Thus, similar to graphene, one can easily extract single or few layers from the bulk compound using mechanical exfoliation or other experimental techniques. Different from graphene, TMDs have an intrinsic band gap [cf. Fig. 1(d)] which makes them especially interesting as atomically thin field-effect transistors (FETs). Furthermore, one can combine different 2D materials to create van der Waals heterostructures [4] with interesting properties.

One key parameter to understand the charge transport in TMDs is the time between two successive scattering events as it determines e.g. the mean-free path and the mobility of the charge carriers. However, the transport scattering time is not easily accessible by experiments. Here, we report a simple method to extract the scattering time for field-effect doping of monolayers and multilayers of MoS_2, $MoSe_2$, $MoTe_2$, WS_2, and WSe_2. More specifically, we calculate the ratio of the Hall mobility to the scattering time $\mu_{\rm Hall}/\tau$ using Boltzmann transport theory within the relaxation-time approximation. Thus, one can easily extract the scattering time by comparing the measured Hall mobility with this calculated ratio. We exemplify the extraction for WS_2 for measurements done by Braga *et al.* in Ref. [5]. We furthermore show that the onset of doping of the different conduction-band minima in TMDs can be determined by a simple conductivity measurement. This allows for an estimation of the energy difference between different minima in the undoped compounds [cf. Fig. 1(d)].

In order to extract the transport scattering time τ from experiments we use the Boltzmann transport equation [6,7] (BTE) to calculate the conductivity tensor and the Hall tensor within the relaxation-time approximation. The conductivity tensor $\sigma_{\alpha\beta}$ in 2D can be written as

$$\sigma_{\alpha\beta}(T;E_F) = \frac{e^2}{(2\pi)^2}\sum_i \int \tau_{i,\mathbf{k}}\, v_\alpha^{i,\mathbf{k}}\, v_\beta^{i,\mathbf{k}} \times\left[-\frac{\partial f_{E_F}(T;\varepsilon_{i,\mathbf{k}})}{\partial\varepsilon}\right] d\mathbf{k}, \qquad (1)$$

where e is the charge of the charge carriers in band $\varepsilon_{i,\mathbf{k}}$ with momentum $\mathbf{k}$, $f_{E_F}(T;\varepsilon)$ is the Fermi function $f_{E_F}(T;\varepsilon) = (\exp[(\varepsilon - E_F)/(k_B T)] + 1)^{-1}$, and $v_\alpha^{i,\mathbf{k}} = 1/\hbar\, \partial\varepsilon_{i,\mathbf{k}}/\partial k_\alpha$ is

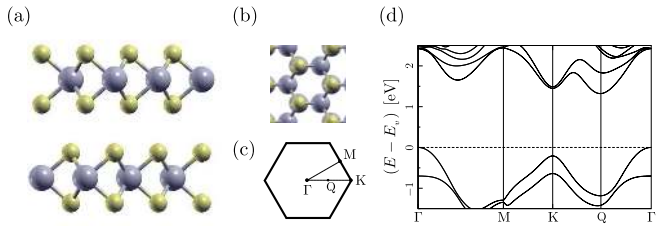

FIG. 1. In the 2H structure of the TMDs the transition-metal atoms of one layer are on top of the chalcogen atoms of the other layer while the atoms within a layer form a hexagonal pattern as can be seen in the (a) side and (b) top view of the structure (gray—transition metal, yellow—chalcogen). The hexagonal 2D Brillouin zone shown in (c) has the special points Γ, M, and K. In the conduction band the TMDs have a minimum approximately halfway between Γ and K (hereby labeled Q point) as shown in the band structure in (d). Its position with respect to the minimum at K depends on e.g. strain and the number of layers. The spin-orbit splitting of the bands at K is larger for the TMDs with tungsten [in (d) the band structure for bilayer WS_2 is shown].

*Present address: Max-Planck-Institut für Struktur und Dynamik der Materie, Luruper Chaussee 149, 22761 Hamburg, Germany; thomas.brumme@mpsd.mpg.de

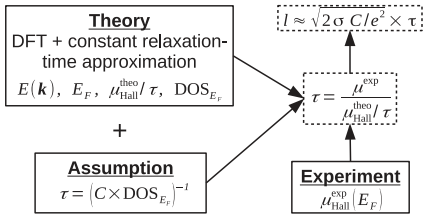

FIG. 2. Flow chart illustrating the procedure used in this paper to calculate the transport properties. First, the band structure is calculated within density-functional theory (DFT) for a doping concentration n as has been implemented in Quantum ESPRESSO [9,10]. The band structure is used as input for BoltzTraP [6] to calculate the transport properties within the constant-scattering-time approximation. Those results can then be used either to extract τ as shown in Fig. 3 or [assuming $\tau = (C \times \text{DOS}_{E_F})^{-1}$] to fit to the experimental mobility $\mu^{\text{exp}}_{\text{Hall}}$ as shown in Fig. 4.

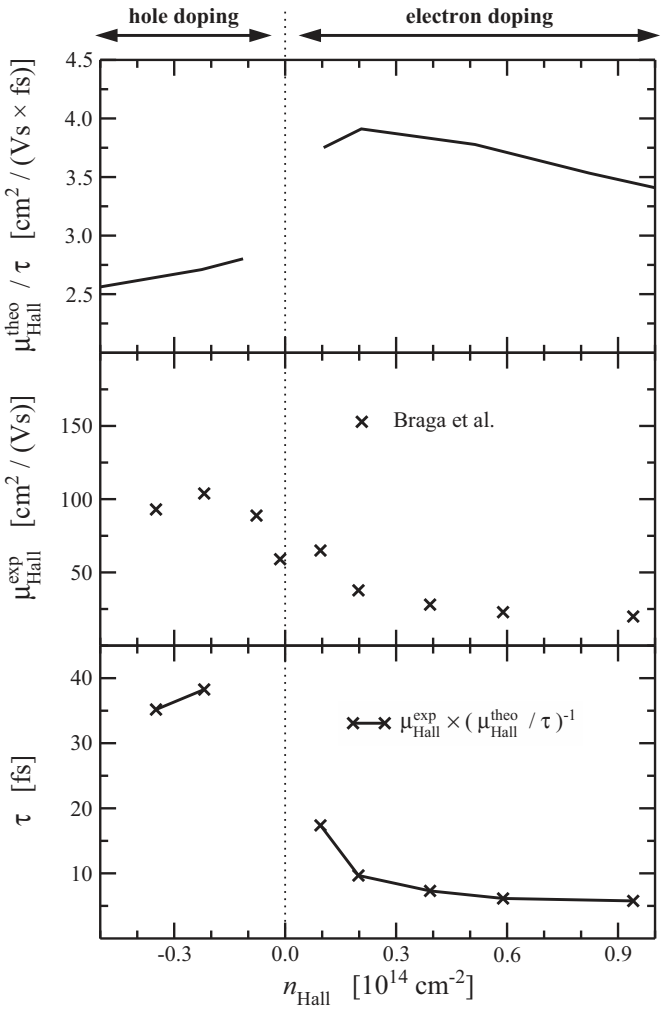

FIG. 3. Extracting the scattering rate for multilayer WS_2. The top panel shows the calculated ratio $\mu^{\text{theo}}_{\text{Hall}}/\tau$ while the measured mobility [5] is given in the middle panel ($T = 300$ K). The bottom panel shows the ratio of both. As the mobility was calculated for doping charge concentrations per unit cell n, which in general are different from the measured concentration n_{Hall} [8], we linearly interpolated the theoretical mobility to extract its value at the experimental doping.

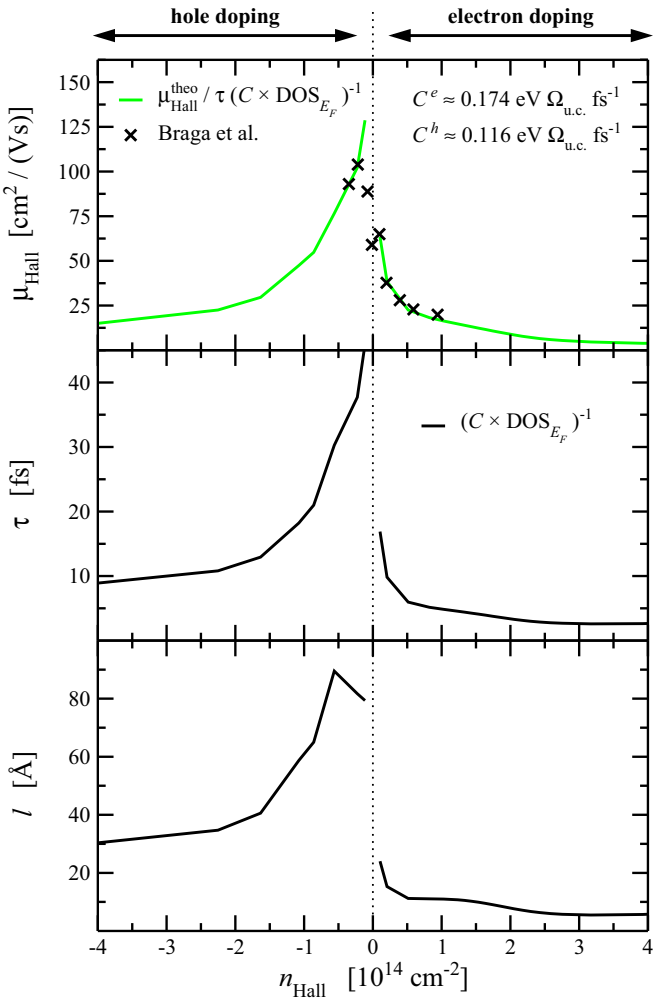

FIG. 4. Extracting the scattering time for multilayer WS_2 at $T = 300$ K using the constant-scattering-time approximation. The experimental data has been taken from Ref. [5]. Assuming $\tau = (C \times \text{DOS}_{E_F})^{-1}$ one can fit the calculated mobility to the measurements (top panel). The resulting scattering time is shown in the middle panel. The corresponding mean-free path, $l \approx \sqrt{2\langle v_x^2\rangle} \times \tau = \sqrt{2\sigma\, C/e^2} \times \tau$, is given in the bottom panel.

the group velocity. The scattering time $\tau_{i,\mathbf{k}}$ depends on both the band index i and the $\mathbf{k}$-vector direction. For crystals with hexagonal symmetry such as TMDs the conductivity has only two independent coefficients [7] (in-plane $\sigma_{||} \equiv \sigma$ and out-of-plane σ_{zz} component). The (in-plane) Hall mobility, which is measured in the experiments, can be written as

$$\mu_{\text{Hall}}(T; E_F) = \sigma(T; E_F)\, R_{xyz}(T; E_F), \tag{2}$$

where $R_{xyz}(T; E_F)$ is the Hall coefficient for the induced electric field along y if the current and the magnetic field are applied along x and z, respectively [6]. Note that $n_{\text{Hall}} \equiv R^{-1}_{xyz}(T; E_F)$ is not the same as the doping charge n and can deviate substantially from the case of an isolated parabolic band. This is due to the specific band structure of the TMDs as shown in Ref. [8]. In the following we drop the "$(T; E_F)$."

For scattering independent of the band index and the wave-vector direction $\tau_{i,\mathbf{k}} = \tau$. Under this assumption, σ/τ, μ/τ, and R_{xyz} are all independent on τ. We can then use the *ab*

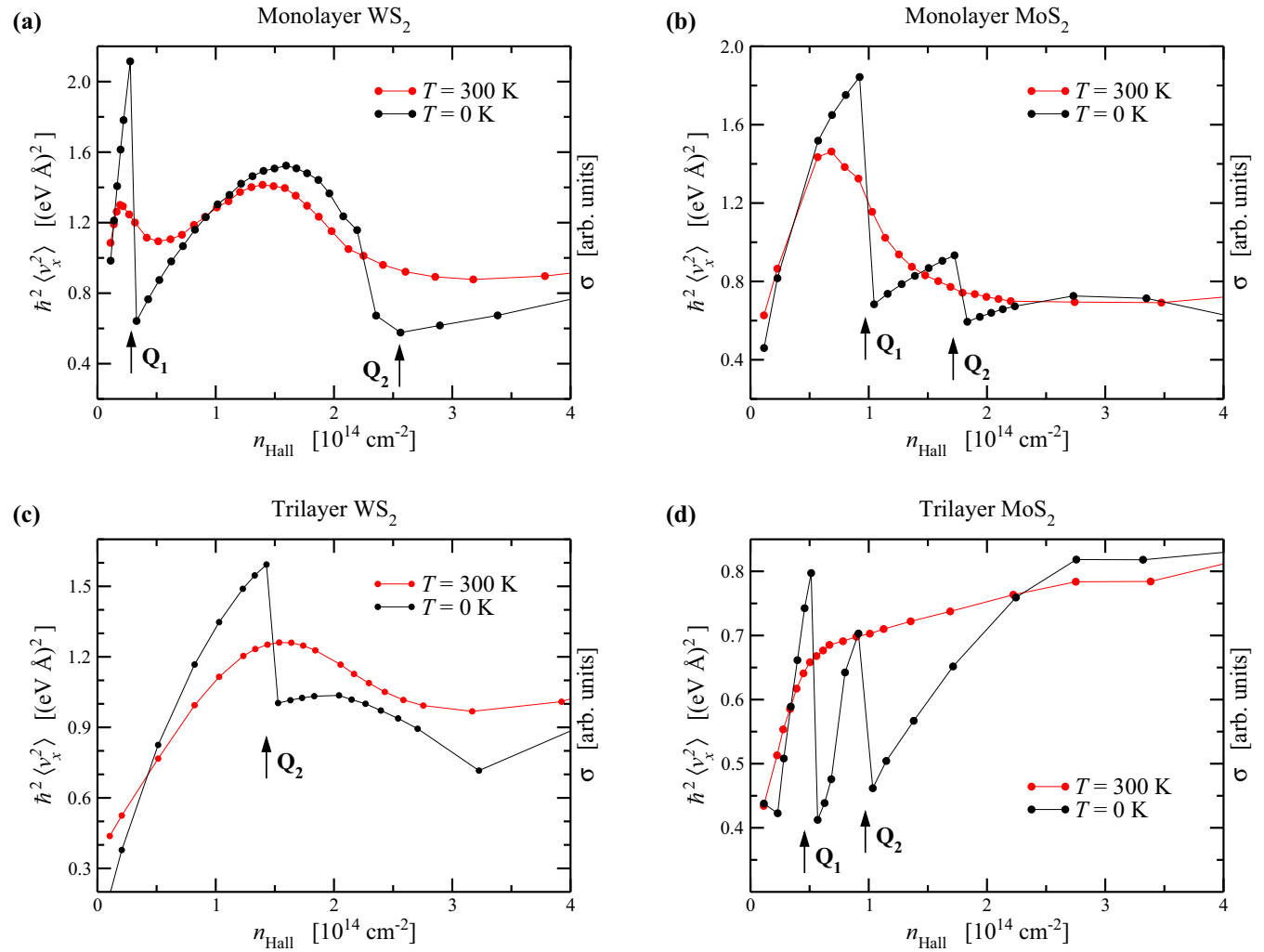

FIG. 5. Average squared velocities $\hbar^2\langle v_x^2\rangle$ of (a),(c) WS_2 and (b),(d) MoS_2 for different number of layers and increasing electron doping. The onset of doping of the different bands at the Q point (approximately halfway between Γ and K, cf. Fig. 1) for $T = 0$ K is indicated by small arrows. For trilayer WS_2 the doping charge first occupies the band at Q and only the onset of doping of the second band at Q is indicated.

initio band structure to calculate the ratio of the theoretical conductivity σ^{theo} and Hall mobility $\mu_{\text{Hall}}^{\text{theo}}$ to the scattering time τ. Our method to calculate those quantities is further clarified in Fig. 2 and the computational details can be found in the Supplemental Material [11]. The ratio of the measured Hall mobility $\mu_{\text{Hall}}^{\text{exp}}$ to the calculated ratio $\mu_{\text{Hall}}^{\text{theo}}/\tau$ can be used to extract the scattering time from the experimental data. Figure 3 exemplifies this extraction for WS_2. The experimental data of Braga *et al.* was measured on a thick sample at $T = 300$ K. We compare this data with the calculations for trilayer WS_2 which is a good approximation for nanolayers with more than three layers and doping larger than $n > 10^{13}$ cm^{-2} as shown in Ref. [8]. The scattering time thus extracted decreases with increasing doping-charge concentration n_{Hall} as shown in the bottom panel of Fig. 3. Furthermore, electrons are scattered more frequently than holes. Hole and electron mobilities are still comparable due to the much higher effective mass of holes at the Γ point as compared to the mass of electrons in the conduction band [12].

The assumption of constant scattering time is not a far-fetched simplification. In fact, for constant scattering matrix elements one can show that the scattering rate $1/\tau$ is proportional to the density of states (DOS) at the Fermi energy. This is also true for electron-phonon interaction if the phonon energy is negligible with respect to the Fermi energy. Accordingly, because of Matthiessen's rule, the total scattering time is directly proportional to the inverse of the total DOS at the Fermi energy $\tau = (C \times \text{DOS}_{E_F})^{-1}$.

In order to obtain the constant C, we use the calculated DOS as outline in Fig. 2 and fit $\mu_{\text{Hall}}^{\text{theo}}/\tau\ (C \times \text{DOS}_{E_F})^{-1}$ to the data of Ref. [5] as shown in the top panel of Fig. 4. For electron doping and hole doping we find $C^e \approx 0.174$ eV $\Omega_{\text{u.c.}}$ fs^{-1} and $C^h \approx 0.116$ eV $\Omega_{\text{u.c.}}$ fs^{-1}, respectively, with $\Omega_{\text{u.c.}}$ the area of one unit cell. The resulting scattering time τ is given in the middle panel. It decreases with increasing doping and saturates for high electron doping at $\tau \approx 3$ fs. Furthermore, in the hole doping case the carriers are less often scattered. The good qualitative agreement between the experimental and the theoretical mobility shows that an energy- and momentum-independent scattering time which is proportional to DOS_{E_F} can be used to estimate the transport scattering time for doping larger than $n > 10^{13}$ cm^{-2}. This indicates that the scattering

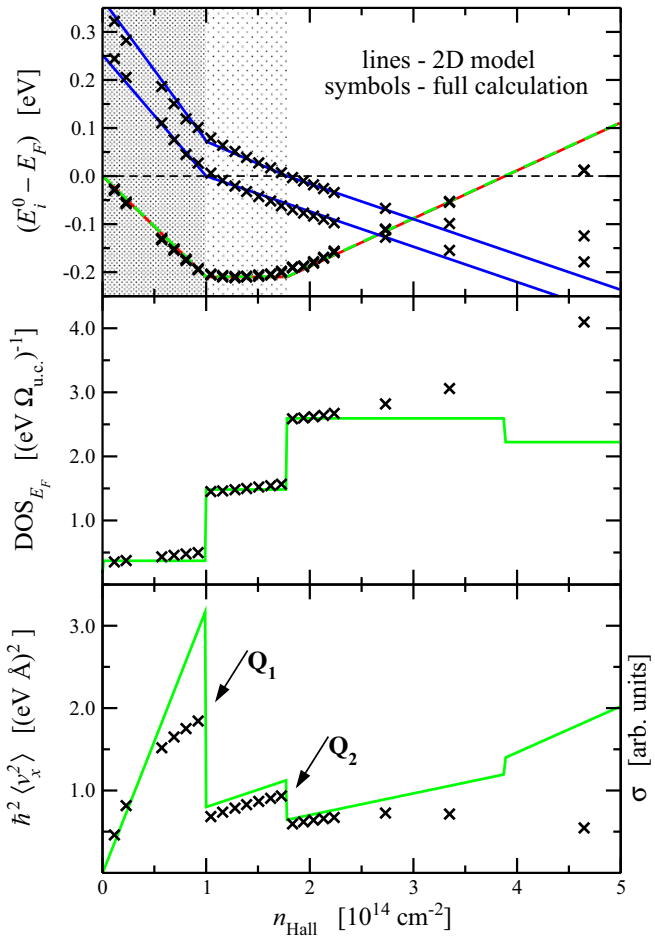

FIG. 6. Comparison between the full *ab initio* calculations using the BTE for monolayer MoS_2 and the simplified model assuming valleys with isotropic, quadratic dispersion. The top panel shows the position of the *ab initio* band maxima as symbols. The positions in the simplified model are shown as solid lines (blue—conduction-band minima at Q, green/red—conduction-band minimum at K; the different shadings indicate the three different phases mentioned in the text). In the middle panel the calculated DOS_{E_F} is compared with the one of the model ($m_K = 0.5\ m_0$ and $m_Q = m_0$). The bottom panel shows the average squared velocity $\hbar^2\langle v_x^2\rangle$ calculated with BoltzTraP as symbols and the one obtained with the model as solid lines. The onset of doping of the spin-orbit-split bands at the Q point for $T = 0$ K is indicated by small arrows.

matrix elements are well approximated by a constant that is independent from the energy and the momentum of the electrons at the Fermi level. Both scattering from neutral defects that do not induce midgap states and electron-phonon scattering from nonpolar phonons, can be modeled with constant matrix elements and could thus explain our findings. Finally, it is important to remark that in calculations the relative position of the minima in the Q and K valleys, their effective masses, and the density of states of the conduction band do depend both on the functional and the lattice parameters used in the calculation (see, e.g., Refs. [12–14]). The good agreement between the experimental and our calculated mobility in Fig. 4 validates our electronic structure in the doping region $0.1 \times 10^{14} < n_{\mathrm{Hall}} < 1 \times 10^{14}$.

Assuming that $\tau = (C \times \mathrm{DOS}_{E_F})^{-1}$, the conductivity is proportional to the average squared velocity of the charge carriers which allows us to estimate the mean-free path. To show this we have to rewrite the in-plane conductivity as follows:

$$\sigma = e^2\,\tau\,\langle v_x^2\rangle\,\frac{1}{(2\pi)^2}\sum_i \int\left[-\frac{\partial f_{E_F}(T;\varepsilon_{i,\mathbf{k}})}{\partial\varepsilon}\right]\mathrm{d}^2\mathbf{k} \quad (3)$$

$$= e^2\,\tau\,\langle v_x^2\rangle\,\mathrm{DOS}_{E_F} = e^2\,\langle v_x^2\rangle\,C^{-1}, \quad (4)$$

where $\langle v_x^2\rangle$ is the average of the squared in-plane velocity over the Fermi surface

$$\langle v_x^2\rangle = \frac{\sum_i \int \left(v_x^{i,\mathbf{k}}\right)^2\left[-\frac{\partial f_{E_F}(T;\varepsilon_{i,\mathbf{k}})}{\partial\varepsilon}\right]\mathrm{d}^2\mathbf{k}}{\sum_i \int\left[-\frac{\partial f_{E_F}(T;\varepsilon_{i,\mathbf{k}})}{\partial\varepsilon}\right]\mathrm{d}^2\mathbf{k}}, \quad (5)$$

with $v_x^{i,\mathbf{k}} = 1/\hbar\,\partial\varepsilon_{i,\mathbf{k}}/\partial k_x$. We furthermore assumed that DOS_{E_F} is given per unit-cell area. Note that it is only possible to define the average squared (in-plane) velocity in such a way due to the hexagonal symmetry. Similarly, using the same approximations, the mobility can be written as $\mu_{\mathrm{Hall}} \propto \langle v_x^2\rangle/n_{\mathrm{Hall}}$. The mean-free path is thus given by $l = \langle v\rangle\,\tau \approx \sqrt{\langle v_x^2 + v_y^2\rangle} \times \tau = \sqrt{2\langle v_x^2\rangle} \times \tau = \sqrt{2\sigma\,C/e^2} \times \tau$. The bottom panel of Fig. 4 shows l for the sample of Braga *et al.* [5]. Since the scattering time for electrons is shorter than for holes the corresponding mean-free path is also much smaller. Holes can travel several unit cells until they are scattered even for doping larger than $n > 1 \times 10^{14}$ cm^{-2}. The mean-free path for electrons on the other hand already becomes as small as three unit cells for $n \approx 0.25 \times 10^{14}$ cm^{-2} and even smaller than two unit cells for $n > 2.4 \times 10^{14}$ cm^{-2}. This short mean-free path demonstrates that we in principle need to go beyond the semiclassical BTE to include quantum effects, which is either an intrinsic problem of WS_2 or just a property of this sample due to a large number of defects. Calculations using more advanced methods such as the nonequilibrium Green's function method are however beyond the scope of this paper, and we thus leave this interesting problem for future investigations. The assumption of a constant scattering time which is proportional to DOS_{E_F} still leads to a good qualitative agreement for $|n| \leqslant 10^{14}$ cm^{-2} as can be seen in the top panel of Fig. 4.

In Fig. 5 we show the average squared velocities $\hbar^2\langle v_x^2\rangle$ [i.e., the conductivity assuming $\tau = (C \times \mathrm{DOS}_{E_F})^{-1}$] for electron doping of the monolayer and trilayer systems of WS_2 and MoS_2. Corresponding curves for hole doping and $MoSe_2$, $MoTe_2$, and WSe_2 can be found in the Supplemental Material [11]. In general, the average velocity first increases and then saturates for higher doping concentrations. Most interestingly, all systems show at least one kink in the average velocity for $T = 0$ K. For higher temperatures these kinks are smeared out until they eventually disappear as can be seen in the case of trilayer MoS_2.

In order to understand the origin of this drop in the conductivity we use a simplified 2D model with isotropic, quadratic dispersion $\varepsilon_{i,k} = \hbar^2k^2/(2m_i) + E_i^0$ with $k^2 = k_x^2 + k_y^2$ and E_i^0 being the bottom of the band i. In the zero-temperature limit, the average squared velocity $\langle v_x^2\rangle = \langle v_y^2\rangle$ can be written as

$$\langle v_x^2\rangle = \frac{\sum_{i,\mathrm{occ}} g_i^v\left(E_F - E_i^0\right)}{\sum_{i,\mathrm{occ}} g_i^v m_i}, \quad (6)$$

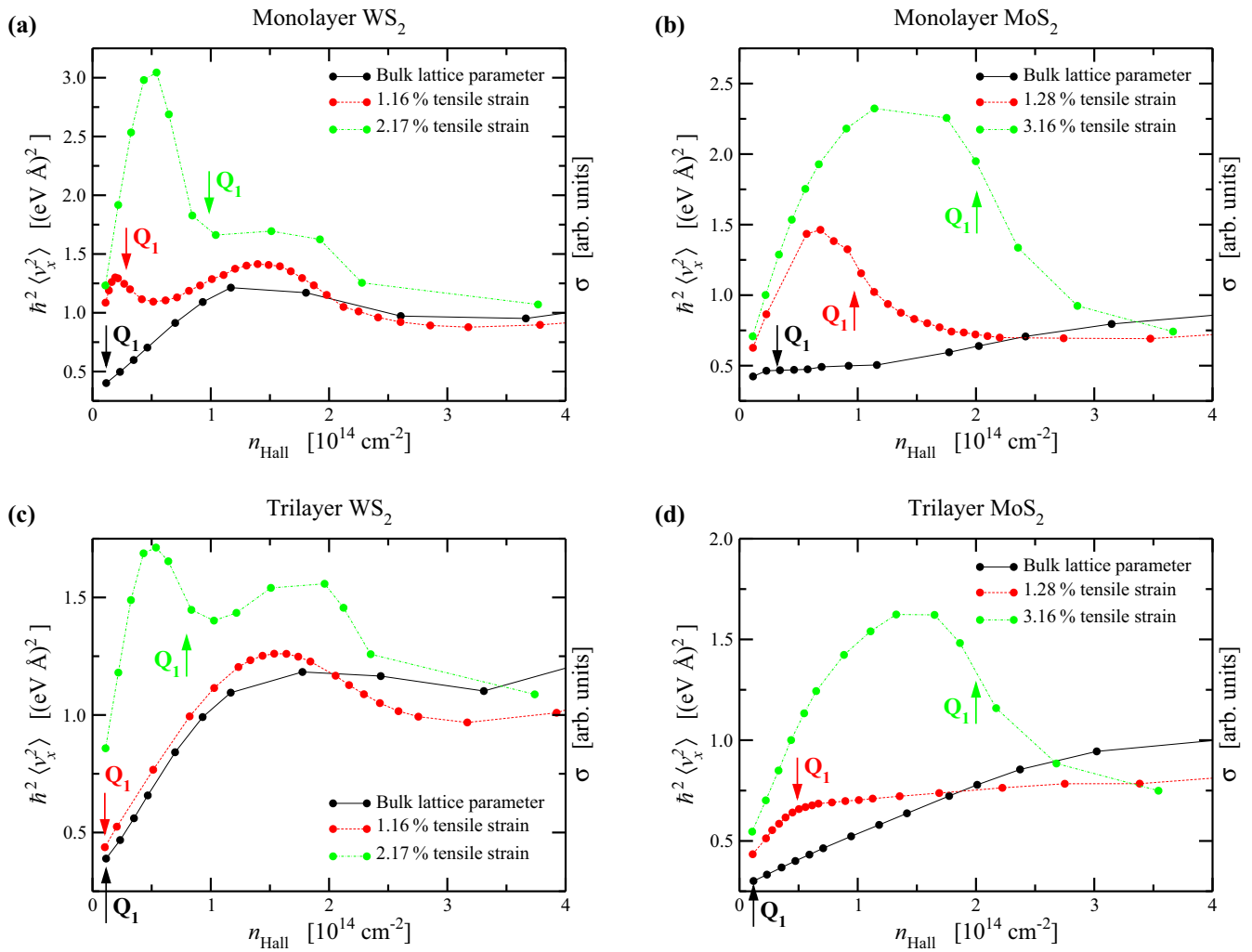

FIG. 7. Average squared velocity $\hbar^2\langle v_x^2\rangle$ of (a),(c) WS_2, (b),(d) MoS_2 for different number of layers with increasing tensile strain $\varepsilon_{xx} = \varepsilon_{yy} \equiv \varepsilon_{||}$ and for $T = 300$ K. The onset of doping of the first band at the Q point (cf. Fig. 1) for $T = 0$ K is indicated by small arrows. The label "Bulk lattice parameter" indicates that the experimental bulk unit cell [15] was used, i.e., $a = 3.160$ Å and $a = 3.153$ Å for MoS_2 and WS_2, respectively. The first strain value is actually the unit cell as relaxed with PBE + D2 while for the second strain value of MoS_2 we increased unit cell to $a = 3.26$ Å as found by Jin *et al.* [16].

with the sums running only over occupied bands i with mass m_i, valley degeneracy g_i^v, and E_F being the Fermi energy.

In Fig. 6 we compare the simplified 2D model with the full *ab initio* calculation for a monolayer of MoS_2. The effective masses in the model of $m_K = 0.5\ m_0$ and $m_Q = m_0$ for electrons at K and at Q, respectively, were determined using DOS_{E_F} of the DFT calculations. The variation of E_i^0 as a function of n_{Hall} has been adjusted to the *ab initio* calculations by assuming three separate phases as indicated by different shading in the top panel of Fig. 6: (i) First only the two spin-orbit split conduction bands at K are filled until (ii) the first band at Q touches the Fermi level and the occupation of the K valleys stays constant. Finally, when the second band at Q starts to get filled, the doping of the K valleys is reduced (iii). For small doping the model agrees well with the *ab initio* results and only for higher doping it starts to deviate. The main error is the assumption of 2D quadratic bands with doping-independent mass which leads to an overestimation of the average velocity. Using the effective mass as calculated by Yun *et al.* [12] ($m_K = 0.483\ m_0$ and $m_Q = 0.569\ m_0$) the deviation between model and *ab initio* calculations would be even larger. Note that including a broadening due to a finite temperature only leads to a smooth decrease of $\hbar^2\langle v_x^2\rangle$ instead of a step close to $n_{\mathrm{Hall}} = 10^{14}$ cm^{-2} but does not decrease the velocity considerably as can be seen in Fig. 5(b). The drop is related to the onset of doping of the Q valley. As apparent in Eq. (6) it is directly proportional to DOS_{E_F}. For doping $n_{\mathrm{Hall}} > 2.5 \times 10^{14}$ cm^{-2} the model shows an increasing average velocity while the velocity is constant in the *ab initio* calculations. These different behaviors are due to the strong nonparabolicity of the conduction bands at Q.

The comparison with the simplified model shows that the kink in the conductivity can be used to determine experimentally the onset of doping of the Q valley in monolayer TMDs and thus the relative position of the conduction-band minimum at Q with respect to the one at K. In calculations this energy difference between K and Q depends on a lot of

parameters (e.g., the level of theory or the unit cell size) which is why one can also find quite different values in literature. Unfortunately, also experiments were up to now not able to give a clear answer since for example ARPES only probes the occupied states or light absorption/emission is much stronger for direct transitions. The results in Figs. 5 and 6 highlight an easy way to determine the onset of doping of the Q valley by a conductivity measurement. This is particular important for superconductivity as the different valleys also exhibit very different electron-phonon coupling [17].

The average squared velocities shown in Fig. 5 support this picture. For a quadratic dispersion in 2D the conductivity (which is the squared velocity) is a linearly increasing function of the doping charge n and has kinks as soon as a new band starts to get doped. The DOS would be constant in this scenario with steps as soon as a new band enters the bias window. The deviation from this 2D behavior is larger for the trilayer systems in which the kink is much less pronounced than in the monolayer case. Furthermore, DOS_{E_F} has a stronger 2D character in trilayer WS_2 than in trilayer MoS_2 [8,11] which is why the former has a small decrease in $\hbar^2\langle v_x^2\rangle$ once the second band at Q gets occupied while the latter does not change at $T = 300$ K.

A second confirmation that the kink is really related to the onset of doping at Q can be found be applying strain to the system. It is well known [12–14] that strain changes the position of K with respect to Q considerably. Furthermore, the influence of strain on the conductivity kink is also important from the experimental point of view as it has been shown that the lattice might relax when going from the bulk to the monolayer limit [16]. Figure 7 shows that the maximum in the average squared velocity (and thus in the conductivity) shifts considerably with applied strain. In both the monolayer and the trilayer systems the kink can shift by as much as $n_{\mathrm{Hall}} = 1 \times 10^{14}$ cm^{-2}. Most interestingly as soon as the measured bulk lattice parameter is used no maximum can be observed at all. A clear kink in the conductivity would thus indicate a relaxation of the lattice as described by Jin *et al.* in Ref. [16]. Note that if the temperature is decreased the maximum in the conductivity will shift to higher doping values due to the smaller broadening of $\partial f_{E_F}(T;\varepsilon_{i,\mathbf{k}})/\partial\varepsilon$, cf. Fig. 5.

In summary, we reported a simple method to extract the scattering time for field-effect doping of TMDs by comparing the measured Hall mobility $\mu_{\mathrm{Hall}}^{\mathrm{exp}}$ with the calculated ratio $\mu_{\mathrm{Hall}}^{\mathrm{theo}}/\tau$. The resulting scattering time can be used to calculate the mean-free path of the charge carriers. We exemplified the extraction for WS_2 for measurements done by Braga *et al.* in Ref. [5]. For this sample we found that the scattering time for holes is larger than those for electrons and that the mean-free path for electrons is much shorter. Even if this indicates the breakdown of the semiclassical BTE for high electron doping of this sample we nevertheless found a good qualitative agreement with experiments. In the Supplemental Material [11] we provide the data needed to extract the transport scattering time by a Hall measurement for monolayers and multilayers of MoS_2, $MoSe_2$, $MoTe_2$, WS_2, and WSe_2. Finally, we also showed that the onset of doping of the different conduction-band minima at Q can be determined by a simple conductivity measurement. As the shape and position of the conductivity peak is influenced by temperature and strain, depending on the experimental conditions it might be difficult, in some cases, to measure a clear peak. However, a conductance saturation/peak has already been seen for MoS_2, [18] WSe_2, [19,20], and SnS_2 [21] and we thus hope that our calculations stimulate more detailed investigations.

We acknowledge Alberto Morpurgo for giving the hint to have a closer look at the conductivity vs doping characteristics. We furthermore acknowledge financial support of the EU FP7 Graphene Flagship Project 604391 and of the French National ANR funds within the *Investissements d'Avenir programme* under reference ANR-13-IS10-0003-01. Computer facilities were provided by PRACE, Centre Informatique National de l'Enseignement Supérieur (CINES), Centre de Calcul Recherche et Technologie (CCRT), and Institut du développement et des ressources en informatique scientifique (IDRIS).

[1] A. K. Geim and K. S. Novoselov, Nat. Mater. **6**, 183 (2007).
[2] D. Jariwala, V. K. Sangwan, L. J. Lauhon, T. J. Marks, and M. C. Hersam, ACS Nano **8**, 1102 (2014).
[3] R. Ganatra and Q. Zhang, ACS Nano **8**, 4074 (2014).
[4] A. K. Geim and I. V. Grigorieva, Nature (London) **499**, 419 (2013).
[5] D. Braga, I. Gutiérrez Lezama, H. Berger, and A. F. Morpurgo, Nano Lett. **12**, 5218 (2012).
[6] G. Madsen and D. Singh, Comput. Phys. Commun. **175**, 67 (2006).
[7] N. Ashcroft and N. Mermin, *Solid State Physics*, Science: Physics (Saunders College, Philadelphia, 1976).
[8] T. Brumme, M. Calandra, and F. Mauri, Phys. Rev. B **91**, 155436 (2015).
[9] P. Giannozzi, S. Baroni, N. Bonini, M. Calandra, R. Car, C. Cavazzoni, D. Ceresoli, G. L. Chiarotti, M. Cococcioni, I. Dabo, A. D. Corso, S. de Gironcoli, S. Fabris, G. Fratesi, R. Gebauer, U. Gerstmann, C. Gougoussis, A. Kokalj, M. Lazzeri, L. Martin-Samos, N. Marzari, F. Mauri, R. Mazzarello, S. Paolini, A. Pasquarello, L. Paulatto, C. Sbraccia, S. Scandolo, G. Sclauzero, A. P. Seitsonen, A. Smogunov, P. Umari, and R. M. Wentzcovitch, J. Phys. Condens. Matter **21**, 395502 (2009).
[10] T. Brumme, M. Calandra, and F. Mauri, Phys. Rev. B **89**, 245406 (2014).
[11] See Supplemental Material at http://link.aps.org/supplemental/10.1103/PhysRevB.93.081407 for the details of the *ab initio* calculations, the ratio of the mobility to the scattering time, the DOS at the Fermi energy, and the average squared velocity for monolayers and multilayers of MoS_2, $MoSe_2$, $MoTe_2$, WS_2, and WSe_2.
[12] W. S. Yun, S. W. Han, S. C. Hong, I. G. Kim, and J. D. Lee, Phys. Rev. B **85**, 033305 (2012).
[13] H. Peelaers and C. G. Van de Walle, Phys. Rev. B **86**, 241401 (2012).
[14] H. Shi, H. Pan, Y.-W. Zhang, and B. I. Yakobson, Phys. Rev. B **87**, 155304 (2013).

[15] N. Podberezskaya, S. Magarill, N. Pervukhina, and S. Borisov, J. Struct. Chem. **42**, 654 (2001).
[16] W. Jin, P.-C. Yeh, N. Zaki, D. Zhang, J. T. Liou, J. T. Sadowski, A. Barinov, M. Yablonskikh, J. I. Dadap, P. Sutter, I. P. Herman, and R. M. Osgood, Phys. Rev. B **91**, 121409 (2015).
[17] Y. Ge and A. Y. Liu, Phys. Rev. B **87**, 241408 (2013).
[18] Y. Zhang, J. Ye, Y. Matsuhashi, and Y. Iwasa, Nano Lett. **12**, 1136 (2012).
[19] H. Yuan, M. S. Bahramy, K. Morimoto, S. Wu, K. Nomura, B.-J. Yang, H. Shimotani, R. Suzuki, M. Toh, C. Kloc, X. Xu, R. Arita, N. Nagaosa, and Y. Iwasa, Nat. Phys. **9**, 563 (2013).
[20] A. Allain and A. Kis, ACS Nano **8**, 7180 (2014).
[21] H. T. Yuan, M. Toh, K. Morimoto, W. Tan, F. Wei, H. Shimotani, C. Kloc, and Y. Iwasa, Appl. Phys. Lett. **98**, 012102 (2011).